Analysis of the Aerodynamic Performance of a NACA 2411 Aerofoil with CFD
4B13 Fluid Mechanics II: Assignment 2

November 15, 2021

1   Domain and Geometry

(a) Flow domain.

(b) Far-field mesh.

(c) Aerofoil mesh geometry.
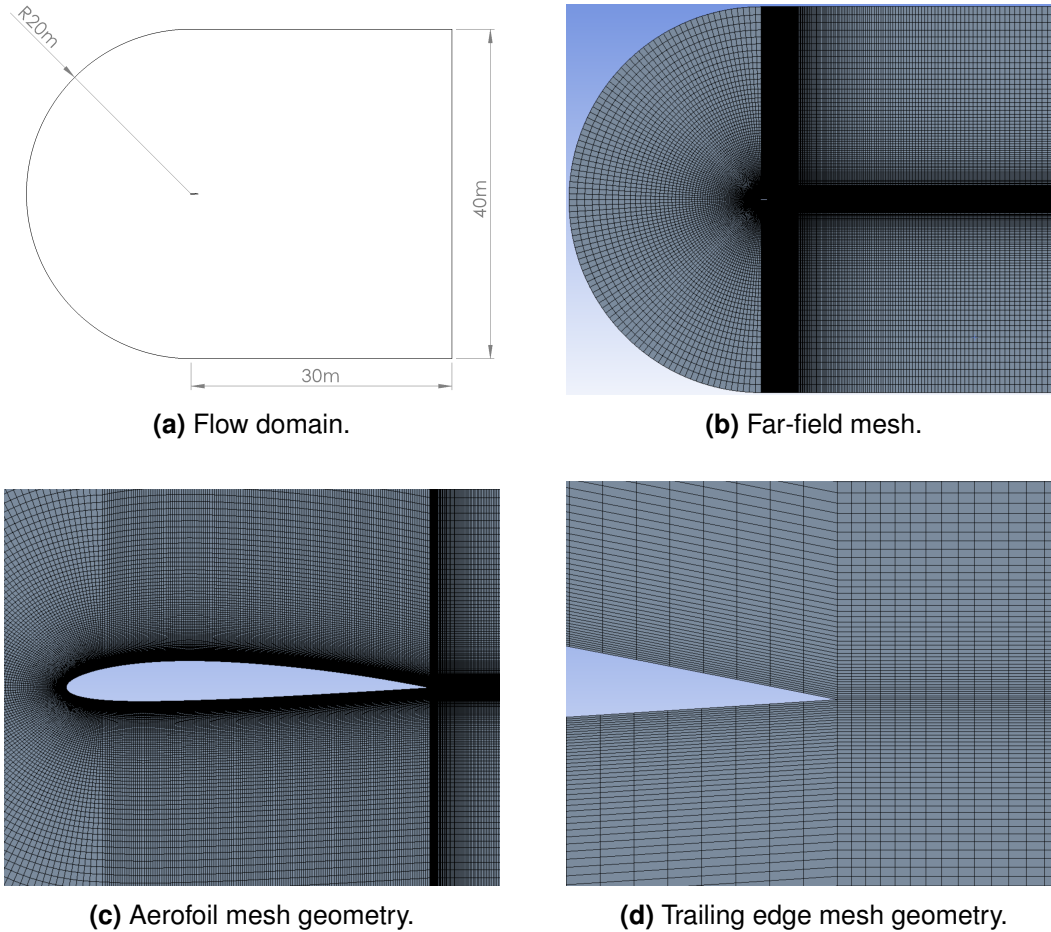
(d) Trailing edge mesh geometry.

Figure 1: Flow domain and mesh geometry.

The flow domain was sized to prevent any wall interactions which could perturb flow variables around the aerofoil such as domain wall boundary layer interaction and the Venturi effect between the domain wall and aerofoil surface. A C-Type mesh was adopted which has the advantage of capturing leading edge curvature without any singularities [1]. Quadrilateral elements were used to make sure air left smoothly from the trailing edge and to ensure low skewness. To capture the important effects of the viscous sub-layer near the aerofoil surface a y^+ mesh layer sizing method [2, 3] was used based on the relation below:

$$y = \frac{\mu y^+}{\rho u_\tau} \qquad u_\tau = \sqrt{\frac{\tau_w}{\rho}}$$

The friction velocity u_τ is directly related to the wall shear stress τ_w experienced by the aerofoil. To obtain the skin friction coefficient C_f the Schlichting formula [4] was used.

$$\tau_w = \mu \left(\frac{\partial U}{\partial y} \right)_{y=0} = C_f \cdot \frac{1}{2}\rho U_\infty^2 \qquad C_f = [2 \cdot log_{10}(Re) - 0.65]^{-2.3}, \quad Re < 10^9$$

$$C_f = 2.5795 \times 10^{-3} \qquad \tau_w = 128.72 \tfrac{N}{m^2} \qquad u_\tau = 0.3591 \tfrac{m}{s}$$

For a mesh with a $y^+ = 5.0$ a first layer thickness of $1.3959 \times 10^{-5} m$ would be used however a layer thickness smaller than this was used to avoid putting the adjacent wall element centroid in the buffer layer [2] as this cell uses a log-law (law of the wall) to model near wall effects but does not model buffer region effects accurately. Using bias factors to concentrate elements near the aerofoil and in the all important wake region allowed the element count to be kept low at roughly $266,000$ elements. Mesh aspect ratio was reasonably okay and an average skewness of 2.3×10^{-2} is well within the limits recommended by ANSYS [5].

Mesh Metric	Min.	Max.	Avg.
Aspect Ratio	1	3701	57
Skewness	1.3×10^{-10}	0.5	2.3×10^{-2}

Table 1: Mesh quality metrics.

2 Simulation Setup

Turbulence Model

The k-ω SST (Menter Shear Stress Transport) turbulence model was chosen for this simulation due to it's robustness. The k-ω SST model combines the k-ϵ model in the free stream which has a good convergence rate and low memory requirements along with the nonlinear k-ω model which exhibits better accuracy than the k-ϵ model in predicting near wall behaviour for flows with strong curvature and flow separation, but is difficult to converge [6, 7].

Physical Constants

$$U_\infty = 10 \tfrac{m}{s} \qquad \rho = 998.2 \tfrac{kg}{m^3} \qquad \mu = 0.0010005 Pa \cdot s \qquad L_C = 1m$$

$$Re = \tfrac{\rho U_\infty L_C}{\mu} = 9.98 \times 10^6 \qquad q_\infty = \tfrac{1}{2} \rho U_\infty^2 = 49,910 Pa$$

Angles of Attack

To accurately assess the aerofoil for it's zero-lift angle of attack and it's behaviour in the stalled region an angle of attack range of $-3°$ to $20°$ was chosen the lower value was based on the $\alpha_{L=0}$ value predicted by thin aerofoil theory and the upper value was based on judgement given the camber of the aerofoil which lowers the angle of attack at which it can operate before the onset of stall. The aerofoil was tested at increments of $1°$ in this range with finer increments implemented close to the stall region, this required overrunning the stall angle and then testing the increment halfway between the stalled and attached angle.

Computational Requirements

As summarised in Table 2, as the angle of attack increased time to solution convergence became longer (convergence criteria was taken to be when solution residuals dropped below 1×10^{-3}) due to the turbulence requiring to resolve a larger range of length scales of turbulent eddies. In particular for angles of attack $\alpha \geq 17°$ convergence of force values was hard to obtain and adjustment of under-relaxation values was required to increase solution stability however this resulted in longer convergence times [8].
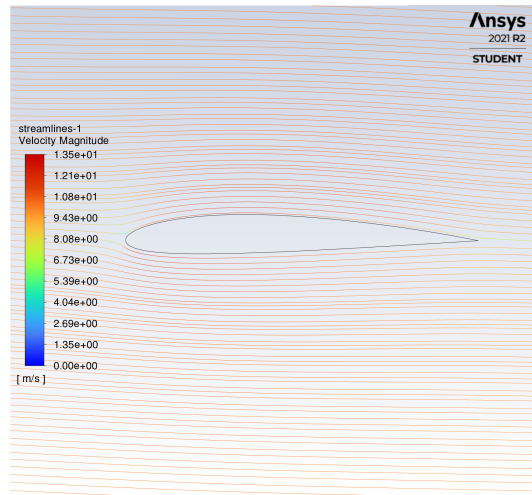
Angle of Attack (α)	Iterations to Convergence
$-3°$ to $7°$	$50 \sim 60$
$7°$ to $15°$	$50 \sim 100$
$15°$ to $20°$	$100 \sim 300$

Table 2: Flow simulation computational load.
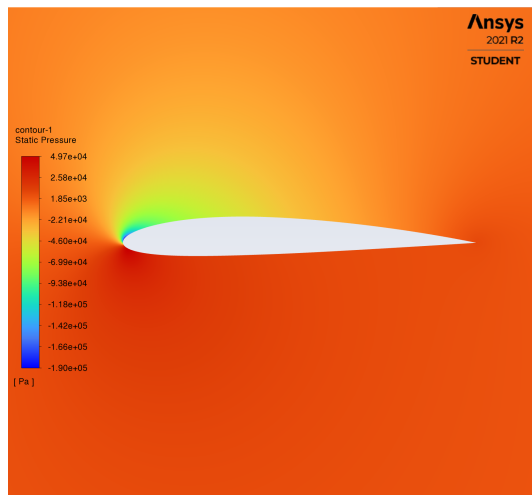
3 Results (Flow Field)
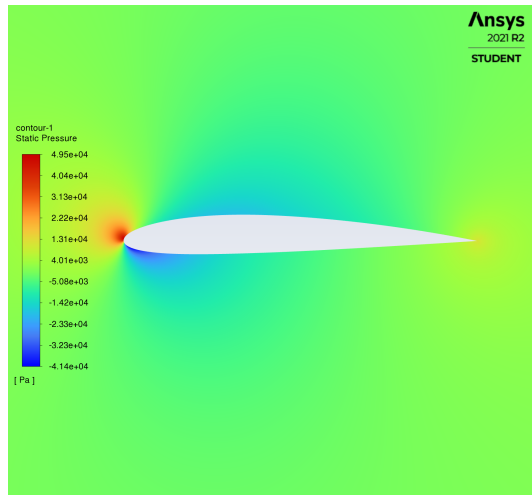
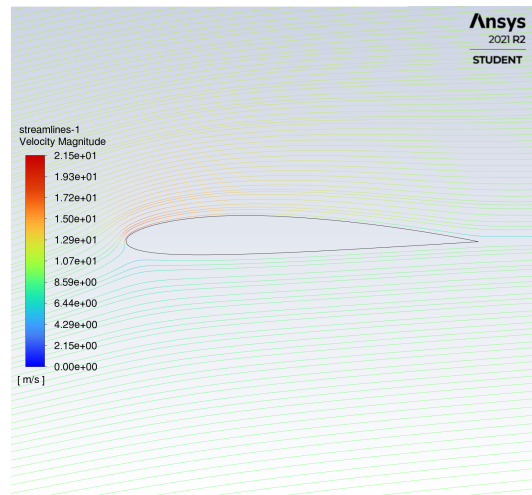**(a)** Static pressure distribution.

(b) Streamlines coloured by velocity.

Figure 2: Near no lift configuration ($\alpha = -2° \simeq \alpha_{L=0}$).
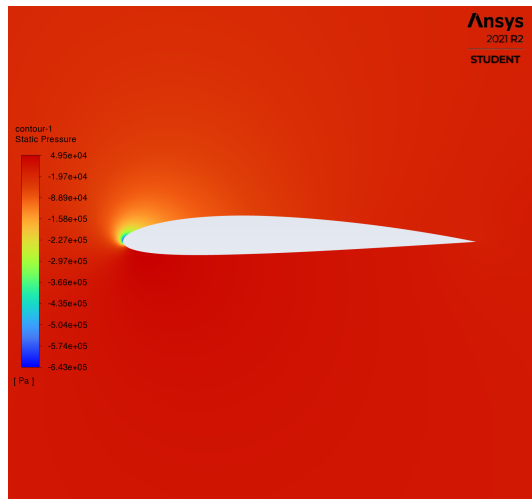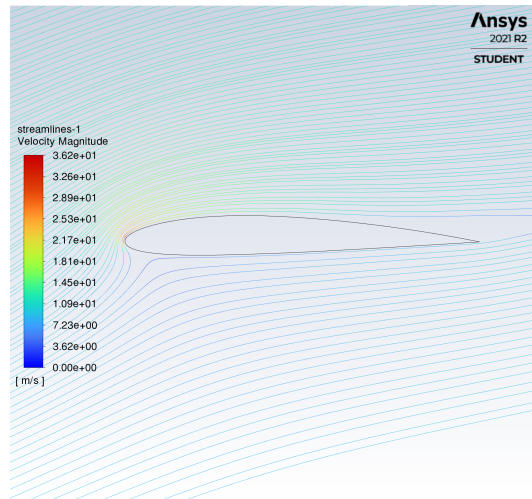

(a) Static pressure distribution.

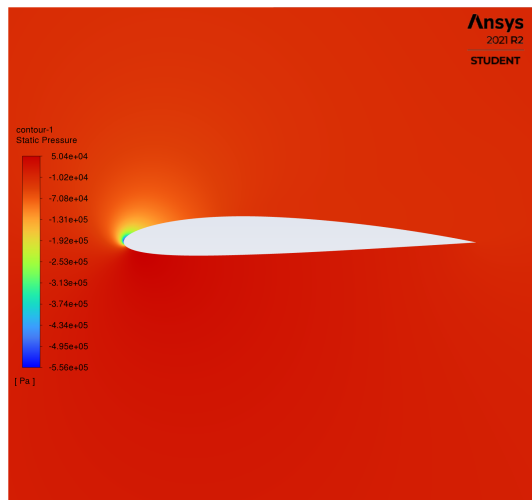**(b)** Streamlines coloured by velocity.

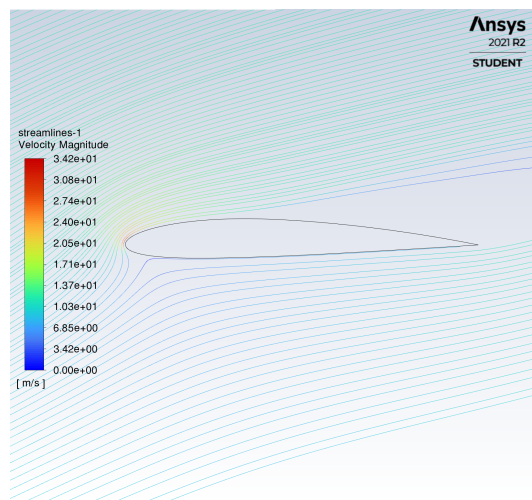**Figure 3:** Moderate lift configuration ($\alpha = 8°$).

(a) Static pressure distribution.

(b) Streamlines coloured by velocity.

Figure 4: High lift configuration starting to separate ($\alpha = 17°$).

(a) Static pressure distribution.

(b) Streamlines coloured by velocity.

Figure 5: Stalled flow ($\alpha = 20°$).

4   Results (Force Coefficients)

Zhukovsky Aerofoil Definition

A NACA 2411 aerofoil is defined by it's thickness ratio of $\frac{t}{c} = \frac{11}{100}$ and camber ratio of $\frac{h}{c} = \frac{2}{100}$ for a Zhukovsky aerofoil theory analysis.

Thin Aerofoil Definition

The mean camber line coordinate definition for a NACA 2411 is shown below along with the transformed and differentiated definition for a thin aerofoil theory analysis.

$$\frac{z}{c} = \frac{1}{8}\left[\frac{4}{5}\frac{x}{c} - \left(\frac{x}{c}\right)^2\right], \quad 0 \leq \frac{x}{c} \leq 0.4 \qquad \frac{dz}{dx} = \frac{1}{8}\left[\frac{4}{5} - 1 + \cos\theta\right], \quad 0 \leq \theta \leq 1.3694$$

$$\frac{z}{c} = \frac{1}{18}\left[\frac{1}{5} + \frac{4}{5}\frac{x}{c} - \left(\frac{x}{c}\right)^2\right], \quad 0.4 \leq \frac{x}{c} \leq 1 \qquad \frac{dz}{dx} = \frac{1}{18}\left[\frac{4}{5} - 1 + \cos\theta\right], \quad 1.3694 \leq \theta \leq \pi$$

The angle of attack resulting in zero lift can be estimated from thin aerofoil theory as being $\alpha_{L=0} \simeq -0.036254684 \simeq -2.08°$.

Force Coefficient Plots

Experimental data for comparison was only available for a NACA 2412 aerofoil and was obtained from [9]. The data was digitized from a graphed format into a tabular format using [10], the data series chosen corresponded to a $Re \simeq 8.9 \times 10^6$.
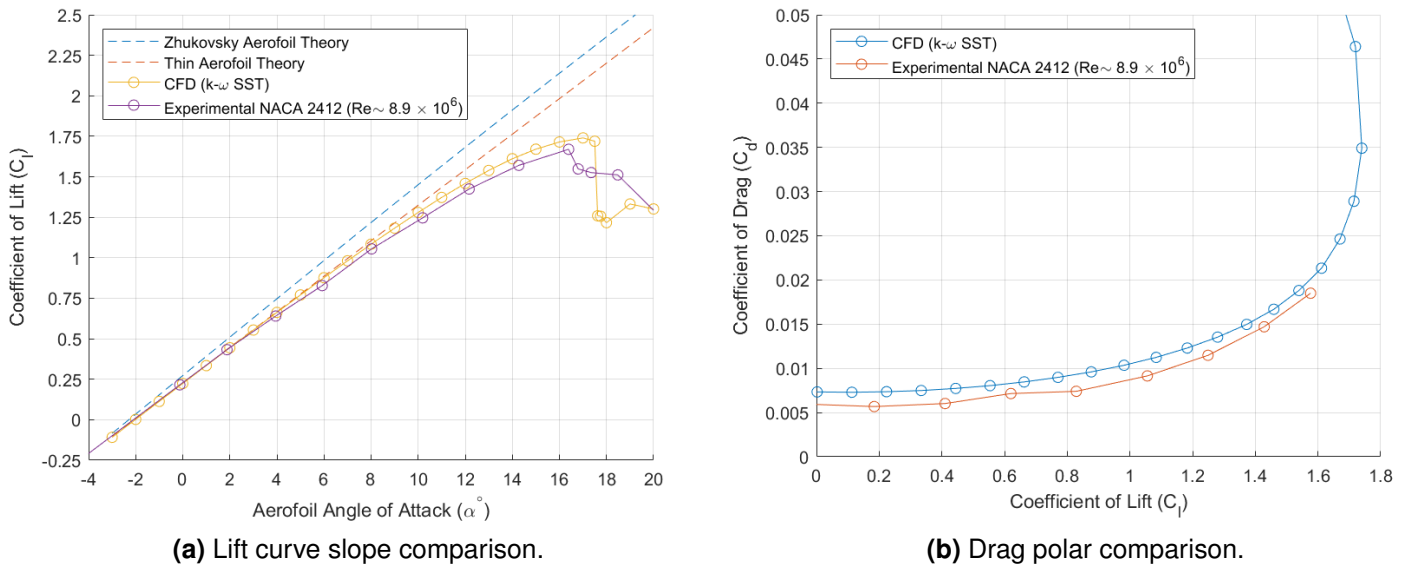

(a) Lift curve slope comparison.

(b) Drag polar comparison.

Figure 6: NACA 2411 aerodynamic characteristics comparison.

5 Assessment

For angles of attack $\alpha \leq 8°$ the CFD simulation agrees well with the experimental data and the lift curve slope provided by the thin aerofoil theory analysis. The Zhukovsky Aerofoil Theory, Thin Aerofoil Theory, CFD simulation, and experimental data all agree on a zero lift angle of attack $\alpha_{L=0} \simeq -2°$.

The CFD simulation and experimental data diverge as the stall angle is reached with a sharp drop in lift seen in the CFD data but not as sharp in the experimental data (Figure 6a). The CFD simulation appears to overestimate the stall angle (however we are comparing with data from a slightly more cambered aerofoil) and overestimates the drag (more likely due to errors in data digitization).

The most important factor is the divergence of the behaviour in the stall region between the CFD and the experimental data. This could be remedied by undertaking a mesh independence study or using adaptive meshing techniques to capture turbulence details. CFD numerics could be adjusted (under-relaxation, SIMPLE solver) further to enhance solution stability [8]. A crude method would be to take iteration averaged quantities.

Fundamentally the problem lies in that the aerodynamic forces are unsteady in turbulent flows as seen in Figure 7. If computational cost is no constraint the direct numerical simulation (DNS) method will yield highly accurate results due it not relying on turbulence modelling but rather resolving numerically all of the turbulent scales present on the Kolmogrov scale [6]. However a more balanced approach would be to use perhaps detached eddy simulation (DES).
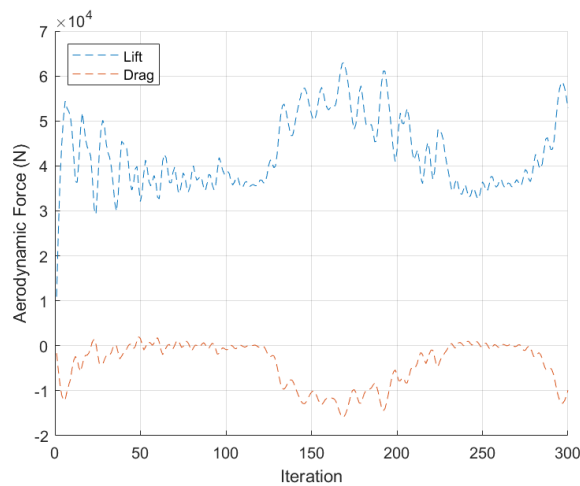
Figure 7: Lift and drag for each simulation iteration ($\alpha = 20°$).

References

[1] Ravindra Krishnamurthy. *The Art and Science of Meshing Airfoils*. November 2017. URL: `https://blog.gridpro.com/the-art-and-science-of-meshing-airfoils/` (visited on 14/11/2021).

[2] *ANSYS FLUENT 12.0 User's Guide - 12.3.1 Near-Wall Mesh Guidelines*. URL: `https://www.afs.enea.it/project/neptunius/docs/fluent/html/ug/node410.htm#sec-guidelines-wf` (visited on 14/11/2021).

[3] *What y+ should I use? Part 3 – Understanding impact of Y+ and number of prism layers on flow resolution — Computational Fluid Dynamics (CFD) Blog – LEAP Australia & New Zealand*. URL: `https://www.computationalfluiddynamics.com.au/y-plus_part3_understanding-impact-of-y-and-number-of-prism-layers-on-flow-resolution/` (visited on 14/11/2021).

[4] Hermann Schlichting. *Boundary-Layer Theory*. New York: McGraw-Hill, 1979. ISBN: 978-0-07-055334-7.

[5] *ANSYS FLUENT 12.0 User's Guide - 6.2.2 Mesh Quality*. URL: `https://www.afs.enea.it/project/neptunius/docs/fluent/html/ug/node167.htm` (visited on 14/11/2021).

[6] Stephen B. Pope. *Turbulent Flows*. Cambridge, UK: Cambridge University Press, 2011. ISBN: 978-0-521-59886-6 978-0-521-59125-6.

[7] Florian Menter. "Two-equation eddy-viscosity turbulence models for engineering applications". In: *AIAAJ* 32.8 (August 1994). DOI: `10.2514/3.12149`.

[8] *ANSYS FLUENT 12.0 User's Guide - 26.3.2 Setting Under-Relaxation Factors*. URL: `https://www.afs.enea.it/project/neptunius/docs/fluent/html/ug/node786.htm` (visited on 14/11/2021).

[9] Ira H. Abbott, Albert E. Von Doenhoff and Louis Stivers. *Summary of Airfoil Data*. Tech. rep. 824. Langley Field, Virginia: National Advisory Committee for Aeronautics, January 1945. URL: `https://ntrs.nasa.gov/citations/19930090976` (visited on 14/11/2021).

[10] Ankit Rohatgi. *WebPlotDigitizer*. URL: `https://apps.automeris.io/wpd/` (visited on 14/11/2021).